Journal of Materials Chemistry A

ROYAL SOCIETY OF CHEMISTRY

REVIEW

View Article Online
View Journal

Cite this: DOI: 10.1039/d6ta00910g

Mechanochemistry-driven CO_2 conversion under mild conditions

Yan Zhou, [a] Qingjie Li,[b] Junxi Shen,[a] He Zhang,[c] Changqing Li,[c] Huiping Qi,[a] Fen Qiao, [a] Junfeng Wang,[ad] Runnan Guan *[c] and Jong-Beom Baek *[c]

Mechanochemistry, increasingly regarded as a "fourth wave" of chemistry, provides a highly dynamic non-equilibrium route in which impact, shear, friction, and fracture concentrate energy within transient contact zones. By continuously renewing defect-rich interfaces and intensifying gas–solid mass transfer, mechanochemical processes can enable efficient carbon dioxide (CO_2) activation and conversion under mild conditions. This review surveys mechanochemistry-driven CO_2 conversion from a sustainability-oriented perspective and classifies existing studies into two mechanistically distinct regimes. First, we discuss non-sustainable mechanochemical routes, in which reactive solids (such as light-metal hydrides, hydrogen-storage alloys, alkaline-earth metals, silicate minerals, or stainless-steel milling media) serve as stoichiometric reagents and are consumed during CO_2 transformation. Second, we highlight sustainable mechanocatalytic pathways, where mechanical actions activate CO_2 over reusable catalysts and sustain closed catalytic cycles, as exemplified by Ru-, Ir-, Ni-based, and metal-free systems. Finally, we outline key challenges and future perspectives, focusing on quantitative energy accounting, *operando* identification of active sites and intermediates, product diversification beyond methanation, catalyst exploration, scalable reactor engineering, and artificial-intelligence-assisted catalyst and process optimization. In summary, these perspectives aim to guide the development of mechanochemistry-driven CO_2 conversion as a practical route toward carbon-neutral energy systems.

Received 30th January 2026
Accepted 27th May 2026

DOI: 10.1039/d6ta00910g

rsc.li/materials-a

[a]School of Energy and Power Engineering, Jiangsu University, Zhenjiang 212013, China

[b]Research Center of Fluid Machinery Engineering and Technology, Jiangsu University, Zhenjiang 212013, China

[c]School of Energy and Chemical Engineering/Center for Dimension Controllable Organic Frameworks, Ulsan National Institute of Science and Technology (UNIST), 50 UNIST, Ulsan 44919, South Korea. E-mail: rnguan@unist.ac.kr; jbbaek@unist.ac.kr

[d]School of Energy and Power Engineering, Chongqing University, Chongqing 400044, China

Yan Zhou

Yan Zhou received his PhD degree from Nanjing University of Science and Technology in 2023. He was a joint trained PhD candidate under the supervision of Prof. Jong-Beom Baek at Ulsan National Institute of Science and Technology (South Korea) in 2021 and 2022. He is currently working in Jiangsu University. His research interests are focused on design and synthesis of nanostructured materials for use in energy storage and conversion.

Runnan Guan

Runnan Guan is a post-doctoral research fellow in the School of Energy and Chemical Engineering/Center for Dimension-Controllable Organic Frameworks, Ulsan National Institute of Science and Technology (UNIST), South Korea. He received his PhD degree from University of Science and Technology of China (USTC) in 2021. His research interests focus on mechanochemistry-driven small-molecules conversions.

1. Introduction

Anthropogenic carbon dioxide (CO_2) emissions from industrial activities and fossil fuel combustion have intensified global climate change, manifesting in global warming, rising sea-levels, ocean acidification, and increasing climatic instability.[1–5] These impacts pose severe environmental risks and hinder progress toward net-zero carbon goals. Accordingly, effective strategies to reduce atmospheric CO_2 are urgent, including minimizing emissions *via* clean and renewable energy technologies, capturing and storing CO_2, and converting it into value-added fuels and chemicals.[6–10] Among these approaches, CO_2 conversion has attracted sustained interest because CO_2 is not only a dominant greenhouse gas but also an abundant C_1 feedstock.[11–13] Efficient CO_2 utilization can simultaneously mitigate greenhouse gas emissions and enable the sustainable production of high-value chemical and energy carriers, thereby accelerating the transition toward carbon neutrality.[14–16]

A central challenge in CO_2 conversion is its intrinsic chemical inertness, originating from the strong C═O bonds (bond dissociation energy > 750 kJ mol^{-1}).[17,18] This imposes substantial kinetic barriers, requiring elevated temperatures, high pressures, or highly advanced catalysts to achieve practical conversion rates.[19,20] Although significant progress has been made in thermocatalytic,[21–23] electrocatalytic,[24–26] and photocatalytic[27–29] CO_2 reduction, large-scale implementation remains limited by high equipment costs, demanding operating conditions, and complex reaction mechanisms.[30,31]

Against this backdrop, mechanochemistry, widely regarded as the "fourth wave" of chemistry following thermochemistry (heat), electrochemistry (electricity), and photochemistry (light), offers a distinct reaction paradigm driven by dynamic mechanical inputs (collision, shear, friction, and fracture).[32,33] These processes access highly non-equilibrium environments and continuously regenerate defect-rich interfaces.[34–36] By alleviating kinetic constraints inherent to conventional routes, mechanochemistry has emerged as an attractive alternative for CO_2 activation and conversion under mild conditions.[37–39] In high-energy ball milling, repeated collisions create transient local extremes in pressure and temperature, accelerate C═O bond activation, promote defect formation, and enhance gas–solid contact.[40,41] Such features enable the reaction pathways that are difficult or even inaccessible *via* traditional methods, thereby overcoming the kinetic barriers associated with CO_2 without the need for elevated temperatures.[42–44]

Mechanochemically driven CO_2 conversion is an integral component of gas-involved mechanochemistry, a specialized field where gaseous reactants participate directly in ball-milling-induced transformations. Although less extensively explored than solid- or liquid-phase mechanochemistry, this area has already demonstrated broad compatibility with diverse gases, including hydrogen (H_2), oxygen (O_2), carbon monoxide (CO), CO_2, and hydrogen cyanide (HCN). Most notably, it enables demanding transformations such as the direct synthesis of ammonia from nitrogen (N_2) and H_2 under remarkably mild conditions.[45–48]

Recent advances using ball milling have demonstrated that mechanochemistry can convert CO_2 into carbonaceous products including stable metal carbonates and fuels such as methane (CH_4) under mild conditions. Compared with CO_2-integrated thermochemical pathways, such as biomass pyrolysis, gasification, and hydrothermal processing, which generally rely on high-temperature gas-phase equilibrium reactions to improve carbon utilization efficiency, mechanochemistry-driven CO_2 conversion proceeds through mechanically induced non-equilibrium solid–gas interactions under near-ambient bulk conditions.[37,49,50] This distinction highlights mechanochemistry as a complementary CO_2 valorization strategy, offering unique opportunities for mild-condition operation and the exploration of unconventional reaction pathways.

Presently, mechanochemistry-driven CO_2 conversion can be broadly classified into two conceptual regimes (Fig. 1). In the non-sustainable regime, reactive solids (such as light-metal hydrides, hydrogen-storage alloys, alkaline-earth metals, silicate minerals or stainless-steel milling media) serve as stoichiometric reagents that undergo chemical reactions with CO_2 and are consumed during the conversion.[30,51–53] In the sustainable regime, by contrast, mechanical energy activates adsorbed CO_2 and H_2 over reusable catalysts (*e.g.*, Ru-, Ir-, and Ni-based, and metal-free mechanocatalysts) without net consumption of the solid phase. This enables closed catalytic cycles and facilitates continuous operation.[37,41,54,55]

Despite rapid progress in mechanochemistry, existing reviews have mainly focused on its roles in organic synthesis, materials preparation, and general mechanistic features, consequently, a sustainability-oriented framework for mechanochemistry-driven CO_2 conversion remains underdeveloped. In particular, prior discussions have rarely distinguished between two fundamentally different reaction regimes: (1) non-sustainable pathways, in which reactive solids act as stoichiometric reagents and are progressively consumed during CO_2 conversion, and (2) sustainable mechanocatalytic pathways in which mechanical input continuously renews active sites on

Jong-Beom Baek

Jong-Beom Baek received his PhD degree from University of Akron (USA, 1998). He is currently a distinguished professor/director at the School of Energy and Chemical Engineering/Center for Dimension Controllable Organic Frameworks, Ulsan National Institute of Science and Technology (UNIST) in Ulsan, South Korea. He was elected as a member of the Korean Academy of Science and Technology (KAST) in 2021. His current research interests include the mechanochemical synthesis of materials for sustainable applications.

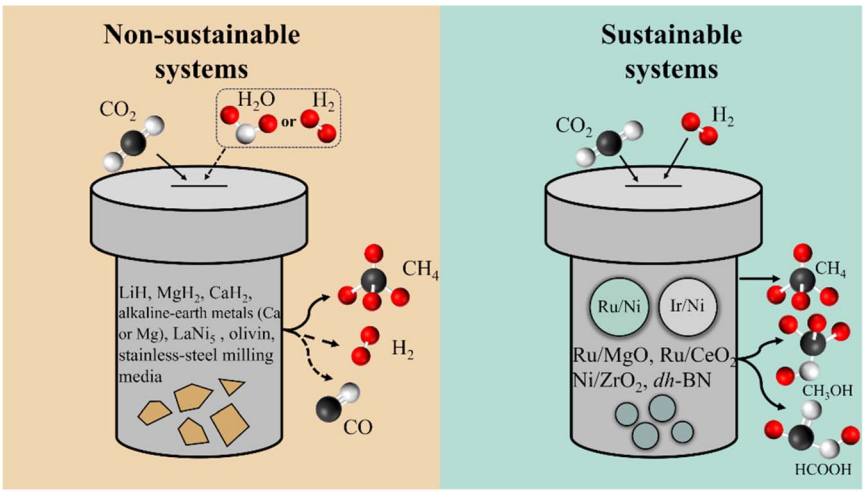

Fig. 1 Classification of mechanochemical CO_2 conversion systems.

reusable catalysts to sustain catalytic turnover without net consumption of the solid phase. Given the increasing urgency of achieving carbon neutrality and the growing recognition of mechanochemistry as a sustainable synthetic paradigm, it is both timely and necessary to assess current progress from a sustainability-oriented perspective.

In this review, we systematically summarize recent advances in mechanochemistry-driven CO_2 conversion. We first examine non-sustainable mechanochemical routes, in which reactive solids serve as stoichiometric reagents and are consumed during CO_2 reduction. We then highlight sustainable mechanocatalytic pathways, where mechanical inputs activate CO_2 over reusable catalysts and sustain closed catalytic cycles. Finally, we discuss current challenges and future perspectives to guide the advancement of mechanochemical CO_2 conversion. Ultimately, this review aims to provide timely insights and practical guidance to accelerate the development of mechanochemistry-driven CO_2 conversion toward scalable and carbon-neutral energy technologies.

2. Non-sustainable mechanochemical CO_2 reactions

Non-sustainable routes rely on the stoichiometric consumption of a solid reagent during mechanochemical CO_2 reduction. In these systems, the reactive solid acts not as a stable catalyst precursor or support, but rather as a sacrificial reagent that is progressively consumed during the CO_2 conversion process. The representative studies discussed below are categorized according to the identity of the sacrificial solid, with an emphasis on their reactor configurations, product distributions, and underlying mechanistic hallmarks.

2.1 Metal hydrides

As ionic solids that combine strong reducing power with low density, light-metal hydrides have been explored as sacrificial reductants for mechanochemical CO_2 conversion.[30,31] For example, Dong *et al.* investigated the room-temperature solid–gas reaction of CO_2 with selected light-metal hydrides in a planetary ball mill (QM-3SP4) using a steel milling vessel (inner volume ~70 cm^3) charged with 30 steel balls (6 mm diameter, total mass of ~27 g).[30] Under these conditions, LiH, NaH, MgH_2, or CaH_2 was milled under 0.1–1.0 MPa CO_2 at 350–550 rpm for 1–48 h, and the reaction performance depended strongly on the hydride identity (LiH > MgH_2 > CaH_2, with NaH remained largely inactive toward CH_4 formation), as well as on the milling speed, duration, and CO_2 pressure. Under representative conditions (LiH/CO_2 molar ration = 4; and CO_2 pressure = 0.25 MPa), the ball-milling process produced only H_2 and CH_4 in the gas phase, with a higher CH_4 fraction achieved at

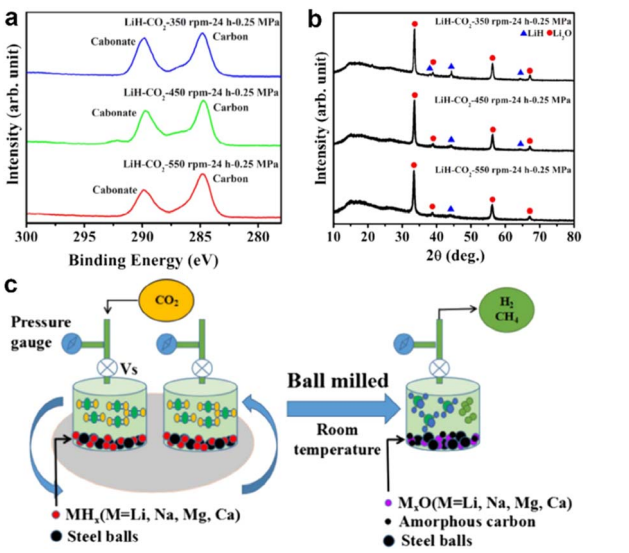

Fig. 2 (a) XPS C 1s spectra and (b) XRD patterns of the solid products obtained after 24 h from the mechanochemical reactions of the LiH_2 with CO_2 (0.25 MPa, LiH_2/CO_2 = 4 mol mol^{-1}) at 350, 450 and 550 rpm. (c) Schematic illustration of CO_2 mechanochemical conversion with light-metal hydrides (alkali or alkaline-earth hydrides). Reproduced with permission.[30] Copyright 2017, Elsevier.

increased milling intensity. X-ray photoelectron spectroscopy (XPS) C 1s spectra (Fig. 2a) exhibited signals attributable to elemental C (~284.5 eV) and carbonate (~290 eV) whereas *ex situ* X-ray diffraction (XRD) patterns (Fig. 2b) revealed the formation of Li_2O. Collectively, these observations support a stoichiometric, reagent-consuming pathway and implicate surface carbon as a key intermediate, consistent with the two-step mechanism proposed in Fig. 2c: (1) impact-assisted CO_2 reduction on MH_x to form M–O/M–CO_3 species along with H_2 and C; (2) subsequent hydrogenation of carbon during continued milling ($C + 2H_2 \rightarrow CH_4$).

By contrast, Pu *et al.* reported a room-temperature mechanochemical route that more explicitly coupled CO_2 conversion with sequestration using simple metal hydrides, including LiH, MgH_2, and CaH_2.[31] In this system, approximately 1 g of hydride was reacted with CO_2 in a ball-milling jar (internal volume ~170 mL), with the gaseous product distribution depending strongly on the CO_2/hydride ratio. At lower CO_2/hydride ratios, CH_4 and H_2 were the dominant gaseous products, whereas CO also appeared and increased in concentration as the CO_2 fraction rose. Meanwhile, the solid products are transformed into metal oxides and carbonates with high CO_2 content, indicating concurrent CO_2 fixation within the solid phase.

2.2 Hydrogen-storage alloys

Beyond metal hydrides, La–Ni-based hydrogen-storage alloys can also serve as solid hydrogen donors for mechanochemical CO_2 conversion in the presence of H_2. Notably, these systems do not function as conventional steady-state catalysts; instead, they undergo mechanically induced structural transformations, in which the parent alloy continuously evolves into dynamically active phases under repeated impact events. For instance, Gemma *et al.* reported that $LaNi_5$ powders were ball milled in a planetary mill (Retsch PM100) using a SUS304 steel vial (50.23 cm^3) and matching balls (10 mm diameter, 10 pieces). Milling was conducted at 250 rpm for 3–27 h under mixed H_2/CO_2 atmospheres, gradually converting CO_2 into CH_4 at near-ambient temperatures, as evidenced by the depletion of CO_2 and the concomitant emergence of CH_4 in gas chromatograph (GC) analyses.[38] Structural characterization revealed that intense mechanical impacts induced pulverization, alloying with Fe/Cr species originating from the milling media, and disproportionation of $LaNi_5$ into nanocrystalline Ni, La-rich oxides, and defective mixed-metal oxide domains. Atom probe tomography (APT) analysis further identified the formation of La- and Fe-containing carboxides and trace hydrocarboxylic species, which likely function as intermediate carbon reservoirs

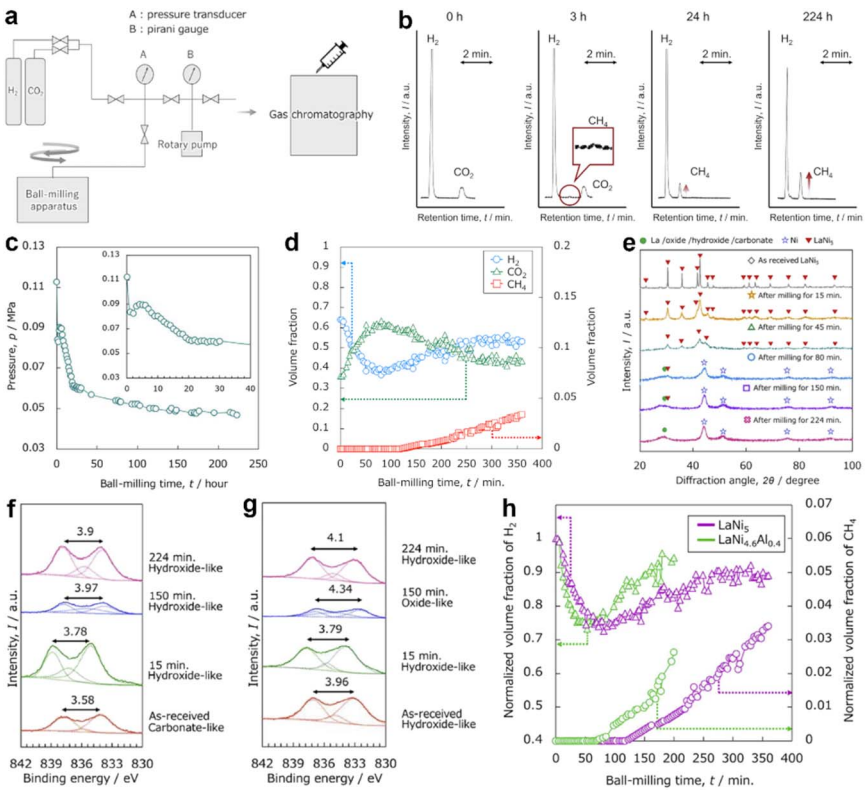

Fig. 3 (a) Schematic illustration of the experimental setup. (b) GC profiles recorded during ball milling of $LaNi_5$ (0.500 g) under a CO_2/H_2 atmosphere at milling times of 0, 3, 24, and 224 h. (c) Gas-pressure evolution during ball milling of $LaNi_5$ powder (0.500 g) under a CO_2/H_2 atmosphere; the inset highlights the initial reaction stage up to 40 h. (d) Evolution of gas-phase volume fractions during mechanochemical CO_2 methanation over $LaNi_5$ under a CO_2/H_2 atmosphere. The H_2 fraction decreases sharply within the first 70 min and then gradually recovers; the combined CO_2 and H_2 fractions sum to unity. (e) XRD patterns of $LaNi_5$ after milling for 224, 150, 80, 45, and 15 min. La $3d_{5/2}$ XPS spectra of $LaNi_5$ after mechanochemical CO_2 methanation at different milling durations after 1 min Ar^+ sputtering at 2 kV: (f) as-measured top surface and (g) sub-surface. (h) Normalized H_2 and CH_4 volume-fraction evolution during mechanochemical CO_2 methanation *via* ball milling of $LaNi_5$ or $LaNi_{4.6}Al_{0.4}$ powder under an H_2/CO_2 mixed atmosphere. Reproduced with permission.[51] Copyright 2022, Elsevier.

during the mechanochemical methanation. The results highlighted a mechanistic scenario in which mechanical forces continuously generate nanoscale metal/oxide/carboxide heterointerfaces, promoting CO_2 activation and hydrogenation without external heating.

Subsequently, Gemma *et al.* reported *in situ* monitoring of mechanochemical CO_2 methanation over La–Ni-based alloy powders subjected to ball milling in a mixed CO_2/H_2 atmosphere.[51] In this system, a vibratory mill (Nissin Giken NEV-MA-8) integrated with a Sieverts-type apparatus was employed, using a SUS304 vial (148 cc) and matching balls (10 mm diameter, 15 pieces) at a vibration frequency of 11.7 Hz. The vibratory mill integrated with a pressure transducer and online GC enabled real-time tracking of gas composition and total pressure during milling (Fig. 3a). The GC results (Fig. 3b) showed that the initial H_2/CO_2 mixture contained no detectable CH_4, while a distinct CH_4 peak emerged after several hours and continuously increased with milling time, demonstrating that CO_2 methanation was driven purely by mechanical activation. *In situ* pressure monitoring during ball milling of $LaNi_5$ (Fig. 3c) exhibited a characteristic three-stage evolution: the pressure dropped sharply within the first hour, increased temporarily between 2 and 4 h, and subsequently decreased again before eventually plateauing after 20 h. This profile indicated that mechanochemical CO_2 methanation proceeded actively for approximately 20 h, after which the system approached a quasi-steady state. Consistently, the normalized H_2 fraction decreased sharply at the onset of milling due to rapid H_2 uptake by $LaNi_5$ and then gradually recovered as hydrogen was released from the bulk hydride and consumed in surface hydrogenation reactions, while CO_2 decreased and CH_4 accumulated (Fig. 3d).

Time-resolved XRD further revealed that $LaNi_5$ initially underwent peak broadening and subsequently disproportionated into metallic Ni and La-based oxides/hydroxides/carbonates, indicating the progressive formation of Ni/La-compound nanocomposites under milling (Fig. 3e). La 3d XPS spectra corroborated the development of hydroxide- and oxide-like La environments at the surface, consistent with $La(OH)_3/La_2O_3$-carbonate ensembles serving as solid carbon reservoirs and CO_2-activating motifs (Fig. 3f and g). Notably, a comparison between $LaNi_5$ and $LaNi_{4.6}Al_{0.4}$ showed an earlier onset and higher rate of CH_4 formation for the Al-substituted alloy (Fig. 3h), underscoring that the hydrogen-storage capacity and hydrogen release kinetics in La–Ni hydrides critically governed the mechanochemical CO_2 methanation pathway.

2.3 Alkaline earth metal-induced hydrogenation of the CaO-captured CO_2

Among non-sustainable mechanochemical CO_2 conversion routes, a mechanistically illuminating example is the selective hydrogenation of CO_2 captured by CaO (*i.e.*, converted to $CaCO_3$) to CH_4 under room-temperature ball-milling conditions, as reported by Mao and co-workers.[53] In this "capture-conversion" scheme, CO_2 was first sequestered by CaO in a cylindrical steel reactor (13.7 mL inner volume) at 650 °C under 5 bar CO_2 to form $CaCO_3$. The resulting $CaCO_3$ was subsequently hydrogenated under mechanochemical conditions by mixing it with 300 mg elemental Ca or Mg. The mixture was milled in a 50 mL planetary ball-mill vessel containing 18 g steel balls (3.14 mm diameter) at 350–600 rpm under 16 bar of H_2 for 2–48 h (Fig. 4a). XRD and solid-state Fourier transform infrared spectroscopy (FTIR) analyses of the Ca-$CaCO_3$-H_2 (16 bar) system milled at 550 rpm identified CaH_2 as a key reaction intermediate. Distinct CaH_2 reflections appeared after 2 h of milling, indicating rapid impact-assisted hydride formation *via* the reaction between Ca and H_2 (Fig. 4b and c). Upon prolonged milling, CaH_2 signals progressively diminished while CaO reflections intensified, consistent with the subsequent consumption of *in situ*-generated CaH_2 by $CaCO_3$ to yield CaO and CH_4. GC and gas-phase FTIR analyses confirmed CH_4 as the only hydrocarbon product under room-temperature milling (Fig. 4d and e).

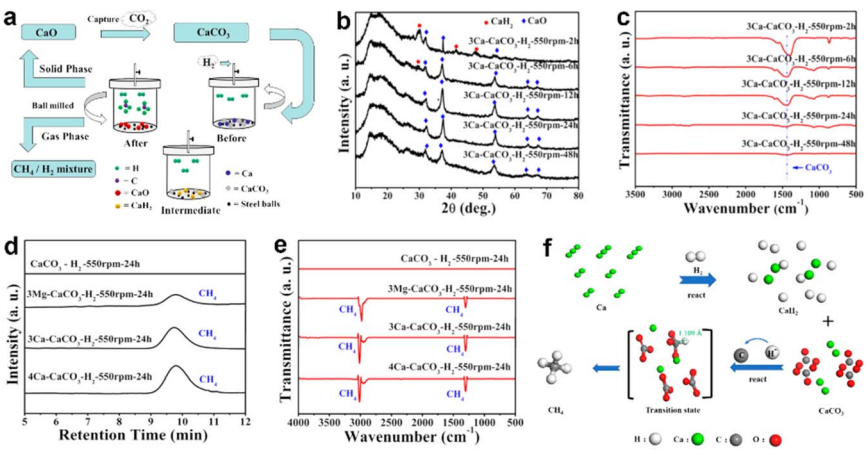

Fig. 4 (a) Schematic depiction of the cyclic process of Ca-induced hydrogenation pOF CaO-captured $CO_2$to CH_4. (b) XRD patterns (c) and solid-state FTIR of solid products from the 3Ca-$CaCO_3$-H_2 (16 bar) system after milling at 550 rpm for different times. (d) GC profiles and (e) FTIR spectra of the gas product from the $CaCO_3$-H_2 (16 bar) and the N (N: Ca, Mg)-$CaCO_3$-H_2 (16 bar) systems after milling at 550 rpm for 24 h. (f) Mechanism diagram of the Ca-induced hydrogenation of the produced $CaCO_3$ to CH_4. Reproduced with permission.[53] Copyright 2022, American Chemical Society.

Notably, Ca outperformed Mg, as the Ca-$CaCO_3$-H_2 system delivered higher methanation activity than the Mg-$CaCO_3$-H_2 system, highlighting the stronger capability of Ca to generate reactive hydride species and promote carbonate hydrogenation under mechanochemical conditions. On this basis, a hydride-mediated mechanism was proposed (Fig. 4f). Mechanical impacts facilitated H_2 activation on Ca, accompanied by CaH_2 formation. The resulting CaH_2 provides highly reactive lattice H^-, which attacked the carbonate carbon to generate a formate-like transition state, consistent with established CO_2 methanation pathways. The intermediate subsequently decomposed to yield amorphous carbon, which was further hydrogenated by H_2 to form CH_4.

2.4 Silicate minerals

Mechanochemically accelerated mineral weathering represents a distinctive non-sustainable route for CO_2 conversion, as the silicate feedstock is consumed stoichiometrically while CO_2 is simultaneously mineralized and, under certain conditions, partially reduced to light hydrocarbons.[56] In contrast to hydrothermal serpentinization, which is thermodynamically favorable yet kinetically sluggish, reactive milling establishes a highly non-equilibrium solid–liquid–gas environment that continuously renews reactive surfaces, enhances dissolution and mass transfer, and enables coupled redox chemistry at near-ambient bulk conditions.[52,56]

In a representative study, Torre *et al.* investigated the mechanically activated reaction between olivine (a natural Fe–Mg silicate) and CO_2 in the presence of water using a SPEX Mixer/Mill 8000 operating at 875 rpm. In this setup, 8 g of an olivine slurry was charged into a 76 cm^3 stainless-steel jar equipped with gas valves and milled with a single 7.50 g steel ball under an initial CO_2 atmosphere of 3 bar.[56] As shown in Fig. 5a, the sealed reactor allowed gas sampling and online analysis during milling. Gas-phase analysis identified CH_4 as the dominant hydrocarbon product, accompanied by minor C_2 species during CO_2-assisted wet milling of olivine (Fig. 5b). Notably, direct comparison with thermal activation under otherwise comparable conditions revealed substantially faster and higher CH_4 yields under milling (Fig. 5c), highlighting the unique ability of mechanochemical activation to intensify interfacial reactions and to promote *in situ* H_2 generation and subsequent CO_2 hydrogenation pathways. In this system, mechanochemically accelerated serpentinization generates H_2 *via* Fe-mediated mineral transformation; the *in situ* generated H_2 subsequently undergoes CO_2 hydrogenation, thereby directly coupling mineral hydration with carbon reduction.

Building on these insights, Gamba *et al.* demonstrated that wet mechanochemical activation of olivine under a CO_2 atmosphere enabled concurrent CO_2 sequestration as $MgCO_3$ and partial conversion to CH_4 at room temperature.[52] The experiments were performed in a planetary ball mill (Fritsch Pulverisette 6) at 500 rpm with a ball-to-powder ratio of 40 : 1, using 2 g of olivine and 0.3 mL of water under initial CO_2 pressures from 0.25 to 1.5 atm. Specifically, short milling durations favored rapid mineral carbonation, whereas prolonged milling

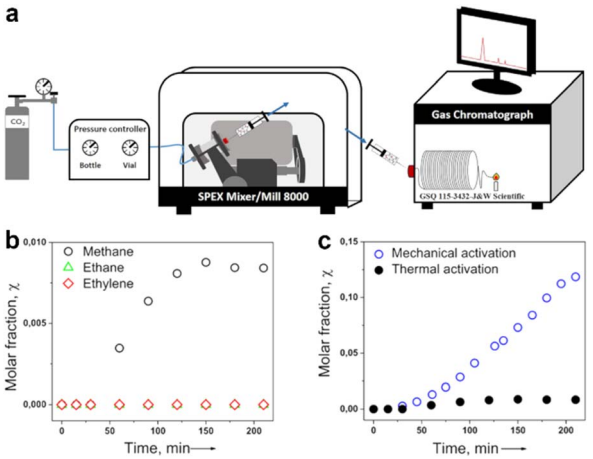

Fig. 5 (a) Schematic of the apparatus used to investigate the mechanochemical reaction. (b) Time-dependent formation of methane, ethane and ethylene from olivine powders reacted with water (6 mL) at 300 °C under 3 bar CO_2. (c) Comparison of CH_4 evolution for wet olivine and CO_2 under mechanical activation (open blue circles) *versus* thermal activation (solid black circles). Reproduced with permission.[56] Copyright 2020, Elsevier.

progressively shifted selectivity toward CH_4, suggesting that mineral carbonation and CO_2 reduction proceeded in parallel while competing for shared intermediates. Compared with dry milling, the presence of water markedly enhanced CO_2 uptake and enabled measurable CH_4/CO formation even at low CO_2 pressures, highlighting the indispensable role of water in sustaining reactive interfacial chemistry. These reactivity trends correlated with continuous microstructural and textural evolution of olivine during wet milling, including dissolution and partial serpentinization, which collectively increased the density of defect-rich, Fe-containing surface domains and thereby enhanced the propensity of the mineral toward both carbonate formation and CO_2 reduction.

2.5 Stainless-steel milling media

Interestingly, a notable non-sustainable system demonstrated that the milling media itself can act as both an active and sacrificial reactant in mechanochemical CO_2 conversion. Sawama *et al.* reported the room-temperature mechanochemical methanation of CO_2 with H_2O in a planetary ball mill (Fritsch Pulverisette Premium Line 7). This setup utilized an 80 mL SUS304 vessel charged with 100 matching balls (~5 mm diameter).[55] Under these conditions, the reaction outcome exhibited a strong dependence on the milling speed: minimal CH_4 was detected between 200 and 800 rpm, whereas near-quantitative CH_4 formation was achieved at 1100 rpm. As illustrated schematically in Fig. 6a, high-energy ball milling induces repeated ball–ball and ball–wall collisions, continuously generating fresh steel surfaces and localized high-energy contact zones. These mechanically activated interfaces enable rapid conversion of the initial CO_2/H_2O mixture into CH_4, accompanied by residual H_2.

The proposed mechanism (Fig. 6b) involves a mechanically sustained redox cycle driven by SUS304 components (Fe, Cr, Ni).

Freshly exposed metal surfaces undergo oxidation by H_2O *via* double solid-state single-electron transfer (SET), producing metal hydroxide/oxide species and H_2. In parallel, CO_2 reacts with H_2O to form carbonic acid (H_2CO_3), which readily captured by metal hydroxide/oxide species to produce metal carbonates (M_xCO_3). Subsequent hydrogenation of these mechanically generated carbonate species by *in situ* produced H_2 yields CH_4 as the dominant product, with only trace C_2 hydrocarbons under optimized milling conditions. Ni species in SUS304 are proposed to facilitate hydrogenation steps, while Fe and Cr primarily sustain metal oxidation and H_2 evolution. Continuous mechanical abrasion is crucial, as it persistently regenerates reactive metal surfaces and ensures intimate contact among H_2, carbonate intermediates, and catalytically active sites. Because the process relies on the continuous oxidation and consumption of the steel surface to sustain H_2 supply and reactive carbonate ensembles, it is therefore classified as non-sustainable.

3. Sustainable mechanocatalytic CO_2 reduction

In contrast to non-sustainable mechanochemical routes dependent on the stoichiometric consumption of reactive solids, sustainable mechanocatalysis aims to establish a closed catalytic cycle in which the solid phase remains largely intact and CO_2 conversion is driven by continuous mechanical activation.

3.1 Noble metal (Ru, Ir)-based mechanocatalysts

Noble metals provide a particularly effective entry point for sustainable mechanocatalytic CO_2 methanation because their intrinsically low barriers for H_2 dissociation and hydrogenation can be further accelerated by mechanically sustained surface renewal.[41,57] Under ball-milling conditions, repeated impacts and shear continuously expose coordinatively unsaturated metal sites, regenerate metal–support interfacial ensembles, and maintain efficient gas–solid contact.[43,58] These dynamic effects are especially beneficial in low-temperature regimes, where conventional thermocatalysis is often limited by sluggish CO_2 activation and gradual deactivation caused by carbon deposition.[58,59] In this context, Ru and Ir-based mechanocatalysts have emerged as two representative noble-metal platforms that translate mechanical forcing into kinetic gains while preserving catalyst recyclability.

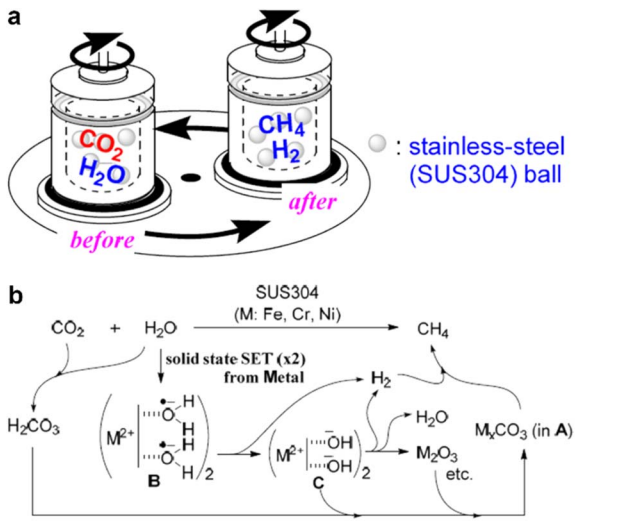

Fig. 6 (a) Quantitative and selective conversion of CO_2 to CH_4 in the presence of water in a stainless steel (SUS304) ball mill. (b) Proposed mechanism for mechanochemical CO_2 reduction. Reproduced with permission.[55] Copyright 2020, Chemical Society of Japan.

One of the earliest benchmarks for Ru-based mechanocatalysts was reported by Mori *et al.* using an Ru catalyst mechanically mixed with MgO (Ru/MgO) in vibrating mill reactor (model MB-1). This setup featured a stainless-steel milling vessel (54.9 mm inner diameter, 115 mm length) charged with 150 stainless-steel balls (10 mm diameter).[43] In a standard experiment, the catalyst was exposed to CO_2/H_2 mixture (100/500 Torr), with the motor speed and vibration amplitude maintained at 1100 rpm and 6 mm, respectively, for a duration of 1 h. Under mechanochemical conditions, Ru/MgO exhibited a pronounced enhancement in CH_4 formation, achieving a CH_4 yield of about 96% at 180 °C, whereas the corresponding thermal operation delivered only about 31% under comparable conditions (Fig. 7a). This improvement was ascribed to persistent shear, compression, and impact that continuously refreshed reactive Ru-containing surfaces and regenerated Ru-MgO interfacial ensembles, while simultaneously suppressing deactivation by disrupting carbonaceous accumulation. Consistent with this interpretation, the apparent activation energy was substantially reduced from 74 to 41 kJ mol^{-1} under mechanocatalytic conditions, indicating that mechanically sustained interface renewal effectively lowers the kinetic barriers associated with CO_2 activation and subsequent hydrogenation steps (Fig. 7b).

In another study, Lv *et al.* developed a mechanochemical strategy to lower the operating temperature of CO_2 methanation using a Ru-CeO_2-grinding catalyst in a custom-built vibration-assisted milling reactor, typically employing ~300 g Fe balls as the milling media and vibration frequencies of 500–1500 rpm, consistently maintaining CH_4 as the predominant product.[41] As shown in Fig. 7c, the Ru-CeO_2-grinding catalyst exhibited higher CO_2 conversion than a simple physical mixture of the same composition operated under static conditions, indicating that mechanochemical activation provides an additional driving force for low-temperature catalysis and thereby reduce the energy demand. Moreover, increasing the reaction pressure to 2 MPa in the static mode resulted in only 0.2% CO_2 conversion, far below the 0.8% obtained under mechanical operation, indicating that bulk pressurization was not the primary origin of the activity enhancement. Infrared imaging indicated that vibration increased the bulk temperature by no more than ~7 °C (Fig. 7d and e), suggesting that macroscopic heating from grinding contributed negligibly to the methanation temperatures employed. Mechanistically, the strong Ru-CeO_2 interaction in Ru-CeO_2-grinding was proposed to enhance

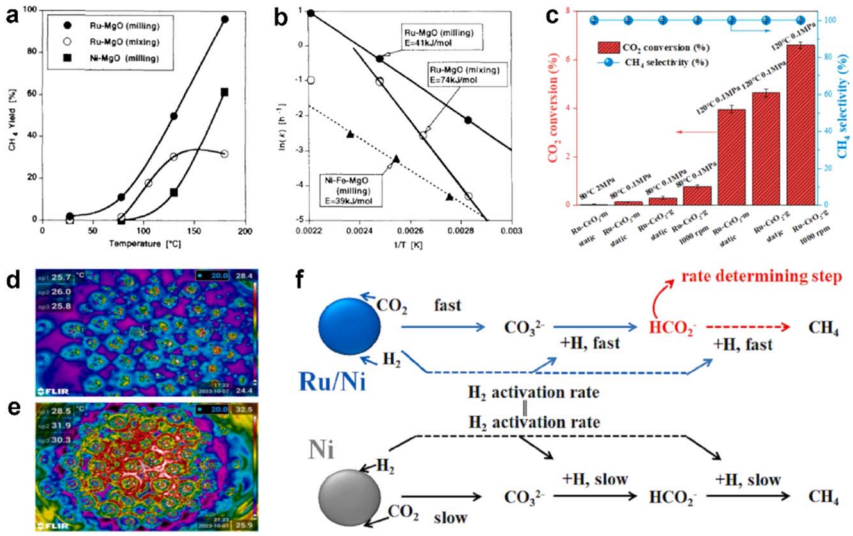

Fig. 7 (a) Arrhenius plots for CO_2 methanation on Ru-MgO and Ni-Fe-MgO catalysts. (b) Effect of temperature on CH_4 yield for Ru-MgO and Ni-MgO catalysts under milling *versus* mixing (1 h). Reproduced with permission.[43] Copyright 1996, Elsevier. (c) The CO_2 methanation performance over Ru(1 g)-CeO_2(5 g)-mix and Ru(1 g)-CeO_2(5 g)-grinding under different reaction conditions. Batch reaction conditions: 300 g Fe balls, 1.5 h reaction time, CO_2: H_2: Ar: N_2 = 2: 8: 5: 85. The temperature variation of Fe balls in vessel (d) before and (e) after 1000 rpm vibration for 4 h *via* infrared camera. Reproduced with permission.[41] Copyright 2025, Elsevier. (f) Proposed pathways for CO_2 methanation on Ni and Ru/Ni catalysts. Reproduced with permissio.[58] Copyright 2023, Elsevier.

H_2 spillover, thereby accelerating hydrogenation of carbonate/formate-type intermediates.

Beyond noble-metal powder mechanocatalysts, a catalyst-on-media architecture has also been demonstrated. In a representative work, Lv *et al.* prepared Ru-modified Ni milling balls (Ru/Ni) *via* a surface deposition strategy that homogeneously disperses trace Ru on metallic Ni balls. This method avoids the formation of detectable Ru nanoparticles, allowing the milling media to function simultaneously as the active catalyst in a custom-built mechanical vibration reactor operated under continuous gas flow.[58] Under typical conditions, utilizing 333 g Ru/Ni balls at a vibration frequency of 1000 rpm and a gas flow rate of a 50 mL min^{-1} ($CO_2/H_2/N_2$ = 1: 4: 45), the catalyst delivered substantially higher CO_2 conversion and CH_4 selectivity than pristine Ni balls while maintaining stable performance for approximately 200 h. Benchmarking against non-vibration operation confirmed a genuine mechanocatalytic promotion, manifested as a reduced apparent activation barrier under mechanical conditions. Mechanistic analysis (Fig. 7f) suggested that CO_2 methanation proceeds through surface carbonate and formate intermediates, with formate hydrogenation governing CH_4 formation. Notably, while Ru/Ni and Ni exhibited comparable H_2 activation capability, Ru primarily accelerated the hydrogenation and turnover of carbonate and formate species at Ru–Ni interfacial ensembles rather than simply enhancing H_2 dissociation, thereby accounting for the markedly improved methanation performance.

For Ir-based mechanocatalysts, Tu *et al.* prepared an atomically dispersed Ir/Ni single-atom alloy by impregnating Ir onto Ni milling balls, thereby integrating the catalyst directly with the grinding medium for CO_2 methanation under continuous gas flow in a custom-built vibration reactor.[54] In this configuration, the Ni balls simultaneously functioned as the catalyst support and kinetic impact medium, with the vibration frequency controlled by the electric motor. The methanation performance was evaluated over 150–450 °C, typically at 800 rpm and a total flow rate of 100 mL min^{-1}. Under these conditions, Ir incorporation markedly enhanced methanation performance relative to bare Ni balls, increasing CO_2 conversion from 8% to 69% and CH_4 selectivity from 57% to 98% at 350 °C. Notably, this system sustained operation for 220 h without observable deactivation, demonstrating the robustness of the SAA structure under mechanical stress. Characterization confirmed atomic dispersion of Ir and its coordination with surface Ni atoms to form an Ir–Ni alloy, in which reduced Ir^0 species exhibited an electronically favorable state while the Ni surface contained coexisting Ni^0 and Ni^{2+} species. Mechanistically, Ni sites served as the primary adsorption centers for CO_2, whereas the Ir–Ni alloy acted as the active sites for H_2 activation and subsequent hydrogenation steps.

3.2 Ni-based mechanocatalysts

Nickel-based catalysts are among the most widely explored materials for thermochemical CO_2 reduction owing to their low cost, earth abundance, and strong catalytic activity.[57,60,61] However, Ni catalysts typically require elevated temperatures to overcome kinetic barriers associated with CO_2 activation and deep hydrogenation. Such harsh conditions often accelerate sintering and carbon deposition, leading to performance degradation.[62,63] Mechanocatalysis offers an alternative route to unlock the reactivity of Ni-based catalysts under milder conditions by continuously renewing Ni surfaces, generating interfacial defects and structural strain, and enhancing both CO_2 capture and intermediate stabilization on reducible oxide supports.[37]

Recently, Guan *et al.* reported mechanochemical CO_2 methanation with unusual performance over a commercially available Ni/ZrO_2 catalyst.[37] The batch mechanochemical process was carried out in a planetary ball-mill (Pulverisette 6, Fritsch) using a 315 mL stainless steel vessel charged with 600 g steel balls. The process can be implemented through three progressive methods: the one-step, two-step, and modified two-step methods (Fig. 8a). In the one-step method, CO_2 and H_2 were continuously consumed to yield CH_4 as the dominant product with only trace C_2H_6, ultimately approaching near-quantitative CO_2 conversion at low temperature of 65 °C (Fig. 8b). Notably, a comparison with continuous thermochemical operation using the same catalyst indicated that the enhanced activity was not simply a consequence of macroscopic bulk heating; whereas thermal operation achieved only 61.3% CO_2 conversion at 500 °C, mechanochemical operation sustained 81.4% conversion and 98.8% CH_4 selectivity at just 15 °C. The two-step and modified two-step methods further demonstrated that mechanochemistry can integrate CO_2 capture and CO_2 conversion within a single catalyst platform, where ZrO_2 primarily contributes to CO_2 capture and Ni provides active site for H_2 dissociation. Notably, highly efficient CO_2 capture was enabled by the high concentration of oxygen vacancies generated under mechanochemical activation, leading to a 75-fold enhancement compared with thermochemical activation (Fig. 8c). Optimization studies further revealed that CO_2 adsorption varied nonlinearly with rotation speed (Fig. 8d), whereas CO_2 conversion increased monotonically with mechanical energy input (Fig. 8e). Mechanistically, the proposed pathway identified oxygen-vacancy-rich ZrO_2 as the CO_2 capture and activation platform (Fig. 8f), on which monodentate carbonate species (*m*-CO_2^*) formed as key intermediates, while Ni supplied efficient H_2 dissociation. Subsequent hydrogen spillover enabled stepwise hydrogenation to formate (*m*-HCOO*) and ultimately CH_4.

3.3 Metal-free mechanocatalysts

Beyond metal-based systems, mechanically enhanced CO_2 hydrogenation has also been demonstrated over defect-engineered metal-free mechanocatalysts. Blair *et al.* reported that defect-laden hexagonal boron nitride (dh-BN), generated *via* high-energy ball milling of h-BN effectively catalyzes CO_2 hydrogenation under mechanically agitated conditions.[64] For the batch mechanocatalytic reaction, 2.5 g of dh-BN was loaded into a stainless-steel reactor containing 440C stainless-steel balls varying diameters, and the system was pressurized with CO_2/H_2 to a total pressure of 685 kPa (393 kPa CO_2 and 292 kPa H_2) at rotation speeds of 60 or 120 rpm. Under these conditions, dh-BN afforded methanol at 20 and 120 °C, whereas formic acid became the dominant product at 160 °C, revealing a distinct temperature-dependent shift in product selectivity (Fig. 9a). Mechanistically, the catalytic activity was attributed to vacancy-mediated activation of CO_2 and H_2, with nitrogen-vacancy sites identified as the most favorable adsorption centers through combined spectroscopic and theoretical analyses (Fig. 9b and c). Importantly, dh-BN functioned as a reusable catalyst rather than a stoichiometric reductant; catalyst deactivation was primarily associated with carbonaceous deposition during cycling rather than irreversible framework consumption (Fig. 9d and e).

4. Challenges and perspectives

This review summarizes recent progress in mechanochemistry-driven CO_2 conversion under mild conditions, emphasizing how mechanical inputs enable CO_2 activation and conversion. Existing studies can be broadly classified into two mechanistic regimes. In the non-sustainable route, reactive solids such as light metal hydrides, hydrogen-storage alloys, alkaline earth metals, silicate minerals or stainless-steel milling media serve as stoichiometric reagents to fix or reduce CO_2, producing

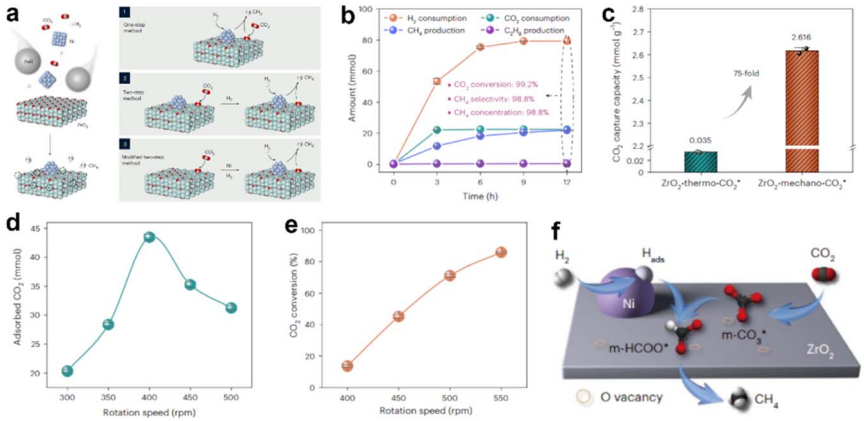

Fig. 8 (a) Schematic overview of one-step, two-step, and modified two-step mechanochemical CO_2 methanation routes. The methanation activities obtained by these three methods were comparable. (b) Time profiles of gas quantities during the one-step process. (c) CO_2 capture capacity of ZrO_2 under thermal *versus* mechanochemical activation. ZrO_2-thermo-CO_2^* was obtained by CO_2 adsorption at 0 °C, and ZrO_2-mechano-CO_2^* was prepared by adsorbing CO_2 at 400 rpm. (d) Amounts of adsorbed CO_2 as a function of rotation speed in the modified two-step method of mechanochemical CO_2 methanation. (e) CO_2 conversion as a function of rotation speed in the modified two-step method of mechanochemical CO_2 methanation. (f) The proposed pathway for mechanochemical CO_2 methanation. Reproduced with permission.[37] Copyright 2025, Nature Publishing Group.

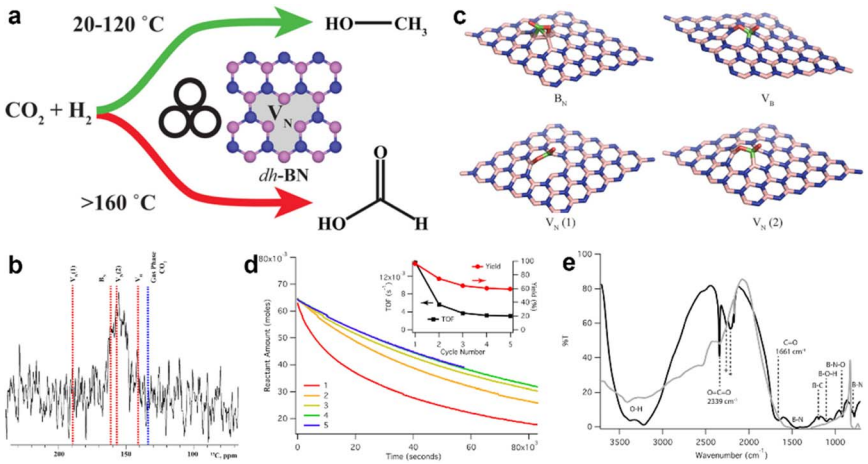

Fig. 9 (a) Schematic illustration of the temperature-dependent product selectivity for CO_2 hydrogenation over dh-BN under mechanochemical conditions. (b) ^{13}C NMR spectrum of CO_2 bound to boron nitride. The red dashed lines denote the calculated chemical shifts for four proposed adsorption configurations, obtained at the B3PW91/D95** level, while the blue dashed line corresponds to gaseous CO_2. (c) Four model structures considered as binding sites for CO_2. (d) The activity of dh-BN for CO_2 reduction with H_2 declines over successive recycling runs and eventually approaches a steady level, consistent with progressive surface coking. At 20 °C, the reduction rate is comparable to that of olefin hydrogenation, although the TOF decreases with each reuse of the catalyst (inset). (e) FTIR spectra of fresh dh-BN (gray) and spent dh-BN (black) reveal the accumulation of carbonaceous species; the bands marked with + and * are assigned to either alkyne or nitrile stretching vibrations. Reproduced with permission.[64] Copyright 2021, American Chemical Society.

carbonates and CH_4 while consuming the solid phase. In the sustainable route, mechanocatalysis sustains closed catalytic cycles on reusable solids, where collision, shear, and friction continuously renew defect-rich metal–support interfaces, promote H_2 dissociation and CO_2 adsorption, and suppress deactivation, thereby enabling selective methanation over Ru-, Ir-, Ni-based, metal-free mechanocatalysts under mild conditions. The effectiveness of these platforms originates from localized energy deposition within transient contact zones, dynamic defect regeneration, and enhanced gas–solid mass transfer, which together lower the apparent kinetic barriers. Despite rapid progress, mechanochemistry-driven CO_2 conversion remains at an early stage, and several key challenges still need to be addressed.

4.1 Standardized quantification of mechanical energy and fair benchmarking

Mechanochemistry-driven CO_2 conversion should be assessed from a process-level energy perspective. Although low bulk operating temperatures are attractive, they do not, by themselves, establish overall sustainability; only a fraction of the supplied electrical energy is converted into chemically productive collisions, while the remainder is dissipated through heat and mechanical damping. The lack of standardized descriptors for mechanical input further limits rigorous comparisons across reactor designs and with established CO_2-conversion technologies. Future studies should, therefore, report complete operating parameters and benchmark performance using both intrinsic and energy-based metrics, including TOF, site-time yield, molar product per kWh, carbon efficiency, and selectivity. Establishing quantitative relationships between operating parameters and collision-energy distributions will be pivotal for fair benchmarking and industrial scale-up. In addition, more quantitative analysis of mechanical energy input and local reaction conditions would bolster mechanistic interpretation and clarify the interplay between mechanochemical activation and thermal effects.

4.2 Operando mechanistic understanding under dynamic non-equilibrium conditions

Mechanocatalysis proceeds through transient contact zones, continuous defect generation, and dynamically evolving interfaces. However, the identity of active sites and dominant reaction intermediates often remains elusive. Addressing these issues requires *operando* toolkits compatible with milling environments, such as online GC/FTIR/mass spectrometry (MS) coupled with pressure tracking, time-resolved XRD for phase evolution, *operando* diffuse reflectance infrared Fourier transform spectroscopy (DRIFTS) and Raman spectroscopy for surface intermediates, and advanced post-mortem mapping *via* APT and aberration-corrected transmission electron microscopy (AC-TEM) to correlate interface evolution with activity. In parallel, mechanically informed microkinetic frameworks and multiscale models should be developed to bridge collision-level events with experimentally observed rates and selectivities.

4.3 Durability, structural evolution, and reactor-material consumption

A key yet under-explored issue in mechanochemistry-driven CO_2 conversion is the long-term stability of reactive materials under continuous milling. In many non-sustainable systems, including hydrogen-storage alloys, metal hydrides, and sacrificial stainless-steel media, reactivity stems from continuous material transformation and consumption rather than from stable catalytic phases. Repeated impacts induce pulverization,

defect accumulation, phase redistribution, and surface oxidation, creating dynamically evolving reactive interfaces. While such evolution is often integral to reaction mechanism, it also complicates assessments of catalyst lifetime and raises practical concerns regarding durability, elemental contamination, and process economics. Systematic studies of long-term stabilities, deactivation mechanisms, and contamination pathways are therefore remain essential for advancing mechanochemical CO_2 conversion toward practical application.

4.4 Catalyst cost and materials selection for sustainable mechanocatalysis

Although noble-metal-based systems, such as Ru- and Ir-based catalysts, have demonstrated promising activity in mechanocatalytic CO_2 conversion, the field is still in its infancy, making a definitive assessment of their practical viability premature. In particular, issues related to catalyst economics, metal loss mechanical wear, and long-term scalability have not yet been systematically examined. Future progress will therefore require not only a deeper mechanistic understanding, but also the development of robust mechanocatalysts based on earth-abundant elements to ensure more practical and scalable implementation.

4.5 Product diversification and catalyst exploration

The product scope in mechanochemistry-driven CO_2 conversion remains relatively narrow. To date, the dominant reduced product reported in mechanocatalysis is CH_4. Therefore, expanding the product envelope toward other C_1 products (such as CO) and higher-value C_{2+} products with high selectivity represents an important yet underexplored direction. Achieving such diversification will require a broader exploration of catalyst compositions and architectures capable of stabilizing key intermediates (*e.g.*, *CO, *CHO, and C–C coupling precursors), together with the deliberate tuning of milling parameters, such as impact intensity, ball size, and gas composition (H_2/CO_2 ratio). Continued efforts in catalyst innovation and mechanochemical process optimization will therefore be critical for unlocking value-added product formation beyond methanation.

4.6 Reactor engineering and continuous operation toward scale-up

Most studies rely on batch milling, which inherently limits throughput. Scale-up requires continuous-flow reactor concepts capable of delivering well-defined mechanical activation while ensuring reliable sealing under pressurized operation, effective temperature management, and the use of wear-resistant materials. Promising directions include ball-milling reactors employing catalytic milling media, designs with circulating grinding elements, and hybrid mechano-thermal configurations. These platforms need to be evaluated using process-relevant criteria including stability over hundreds to thousands of hours, energy efficiency, maintenance requirements, and compatibility with realistic CO_2 feeds and impurities.

4.7 Artificial intelligence for accelerated discovery, control, and scale-up

Artificial intelligence (AI) has significant potential to accelerate mechanochemistry-driven CO_2 conversion by systematically linking the high-dimensional design space to measurable activity, selectivity, and stability. Data-driven models can correlate operating variables (*e.g.*, vibration/rotation frequency, ball size and filling ratio, pressure, gas composition, and temperature) as well as materials descriptors (*e.g.*, particle size, defect density, oxygen-vacancy concentration, and metal–support interaction strength) to optimize catalytic performance, enabling efficient screening and the rapid identification of optimal conditions. At the materials level, AI-guided catalyst discovery can integrate density functional theory (DFT)-derived energetics, microkinetic modeling, and experimentally validated descriptors to propose defect or strain-regulated supports, mechanically robust alloy or single-atom motifs, and catalyst-on-media architectures specifically tailored to dynamic milling environments.

Mechanochemistry-driven CO_2 conversion under mild conditions offers a promising route to overcome kinetic limitations in conventional CO_2 utilization and is emerging as an exciting frontier for catalysis and process intensification. While challenges remain, the distinctive advantages of mechanochemical activation justify intensified efforts in materials design, mechanistic understanding, and scalable reactor engineering. Continued advances along these directions are expected to accelerate the translation of mechanochemical CO_2 conversion toward practical CO_2 valorization aligned with the needs of a rapidly evolving society.

Conflicts of interest

The authors declare no competing interests.

Data availability

No primary research results, software or code have been included and no new data were generated or analysed as part of this review.

Acknowledgements

This work was supported by the National Natural Science Foundation of China (Grant No. 52402117 and 52436005), Natural Science Foundation of Jiangsu Province, China (Grant No. BK20240864), the National Research Foundation of Korea (RS-2023-00221668, RS-2024-00435493, and RS-2024-00466616). The authors also acknowledge support from the InnoCore program of hydro*studio (MSIT: 1.260005.01) at UNIST, dedicated to advanced postdoctoral training.

References

1 J. Ye, N. Dimitratos, L. M. Rossi, N. Thonemann, A. M. Beale and R. Wojcieszak, *Science*, 2025, **387**, eadn9388.

2 B. van der Zwaan, A. Fattahi, F. Dalla Longa, M. Dekker, D. van Vuuren, R. Pietzcker, R. Rodrigues, F. Schreyer, D. Huppmann, J. Emmerling, S. Pfenninger, F. Lombardi, P. Fragkos, M. Kannavou, T. Fotiou, G. Tolios and W. Usher, *Nat. Commun.*, 2025, **16**, 1368.
3 W. Che, S. Zhao, W. J. Byun, T. Tao, J. P. Jeon, Q. Zhao, Y. Shao, J. Li, J. Kim, J. S. Lee and J. B. Baek, *Adv. Mater.*, 2025, **37**, e06961.
4 M. Li, H. Jiang, L. Zhang, X. Yu, H. Liu, A. E. A. Yagoub and C. Zhou, *Ind. Crops Prod.*, 2020, **149**, 112361.
5 Q. Ji, X. Yu, L. Chen, O. P. N. Yarley and C. Zhou, *Ind. Crops Prod.*, 2021, **172**, 114064.
6 B. S. Crandall, M. Naughton, S. Park, J. Yu, C. Zhang, S. Mahtabian, K. Wang, X. Liang, K. Fu and F. Jiao, *Nat. Commun.*, 2024, **15**, 10568.
7 E. Kearns, R. E. Siegel, D. M. D'Alessandro, J.-W. Lee and L. A. Berben, *Chem. Soc. Rev.*, 2025, **54**, 4096–4103.
8 S. Kar, D. Kim, A. Bin Mohamad Annuar, B. B. Sarma, M. Stanton, E. Lam, S. Bhattacharjee, S. Karak, H. F. Greer and E. Reisner, *Nat. Energy*, 2025, **10**, 448–459.
9 L. Zhang, S. Song, H. Zhang and X. Wang, *Chem. Soc. Rev.*, 2026, **55**, 504–555.
10 M. J. Nazir, G. Li, M. M. Nazir, F. Zulfiqar, K. H. M. Siddique, B. Iqbal and D. Du, *Soil Tillage Res.*, 2024, **237**, 105959.
11 G. Long, A. Wang, X. Liu, X. Li, M. Liu, Y. Liu and J. Long, *Angew. Chem., Int. Ed.*, 2025, **64**, e202508217.
12 Y. Guan, Y. Li, Z. Li, Y. Hou, L. Lei and B. Yang, *Adv. Mater.*, 2025, **37**, 2417567.
13 P. Karapapa, S. Mondal, E. Zeglio and B. Das, *Angew. Chem., Int. Ed.*, 2026, **138**, e22226.
14 L. Liu, C. Deng, Y. Xu, X. He, R. Xia, W. Zhu, H. Yao, S. Zhu, X. Kang, X. Tu, D. Shen, J. D. Murphy and R. Lin, *Adv. Funct. Mater.*, 2026, **36**, e13716.
15 M. Jiang, H. Wang, M. Zhu, X. Luo, Y. He, M. Wang, C. Wu, L. Zhang, X. Li, X. Liao, Z. Jiang and Z. Jin, *Chem. Soc. Rev.*, 2024, **53**, 5149–5189.
16 Z. Mustafa, N. Auroona, A. Sarwara and E. Y. Lee, *Green Chem.*, 2026, **28**, 21–36.
17 M. Wu, J. Zhu, Y. Wu, S. Liu, K. Zheng, S. Wang, B. Li, J. Li, C. Liu, J. Hu, J. Zhu, Y. Pan, Y. Sun and Y. Xie, *Angew. Chem., Int. Ed.*, 2025, **64**, e202414814.
18 X. Li, Y. Sun, J. Xu, Y. Shao, J. Wu, X. Xu, Y. Pan, H. Ju, J. Zhu and Y. Xie, *Nat. Energy*, 2019, **4**, 690–699.
19 J. Liu, B. Han, X. Liu, S. Liang, Y. Fu, J. He, L. H. Chung, Y. Lin, Y. Wei, S. Wang, T. Ma and Z. Yang, *Angew. Chem., Int. Ed.*, 2025, **64**, e202417435.
20 D. Suri, S. Das, S. Choudhary, G. Venkanna, B. Sharma, M. A. Afroz, N. K. Tailor, R. Joshi, S. Satapathi and K. Tripathi, *Small*, 2025, **21**, 2408981.
21 S. Verma, M. Kumari, R. Maurya and K. Roy, *Mater. Today*, 2025, **89**, 606–620.
22 H. Wang, C. Gong, X. Xin, S. Li, J. Zhang, B. Ye, X. Bu, J. Li and P. Gao, *Angew. Chem., Int. Ed.*, 2025, **137**, e202516545.
23 K.-M. Kim, J. Mun, G.-N. Yun, Y.-W. You, J. H. Park, J. H. Lee, J. So, H. Shin, J. Kwon, S. Kim, S. Kang, Y. K. Kwon, T. Hyuk Kwon, Y.-S. Bae, G. Lee, S.-J. Kim, Y. J. Kim and H.-T. Kim, *Nat. Commun.*, 2025, **16**, 11617.
24 J. Cheng, L. Chen, Y. Zhang, M. Wang, Z. Zheng, L. Jiang, Z. Deng, Z. Wei, M. Ma, L. Xiong, W. Hua, D. Song, W. Huo, Y. Lian, W. Yang, F. Lyu, Y. Jiao and Y. Peng, *Nat. Commun.*, 2025, **16**, 3743.
25 T. Neves-Garcia, M. Hasan, Q. Zhu, J. Li, Z. Jiang, Y. Liang, H. Wang, L. M. Rossi, R. E. Warburton and L. R. Baker, *J. Am. Chem. Soc.*, 2024, **146**, 31633–31646.
26 Y. Cheng, Q. Li, M. I. B. Salaman, C. Wei, Q. Wang, X. Ma, B. Liu and A. B. Wong, *J. Am. Chem. Soc.*, 2025, **147**, 12438–12448.
27 X. Yin, K. Zhang, C. Xu, Q. Gao, M. Zhang, X. B. Li, H. Q. Peng, C. H. Tung, L. Z. Wu and B. Liu, *Angew. Chem., Int. Ed.*, 2025, **137**, e202508620.
28 R. Zeng, C. Sun, Z. Lin, Y. Li, C. Zhou, S. Zhang, L. Li and S. Guo, *J. Am. Chem. Soc.*, 2025, **147**, 38311–38319.
29 Y. Hu, C. Yu, S. Wang, Q. Wang, M. Reinhard, G. Zhang, F. Zhan, H. Wang, D. Skoien, T. Kroll, P. Su, L. Li, A. Chen, G. Liu, H. Lv, D. Sokaras, C. Gao, J. Jiang, Y. Tao and Y. Xiong, *Nat. Catal.*, 2025, **8**, 126–136.
30 B.-X. Dong, J. Zhao, L.-Z. Wang, Y.-L. Teng, W.-L. Liu and L. Wang, *Appl. Energy*, 2017, **204**, 741–748.
31 K. Pu, Y. Yang, X. Qu, M. Gao, Y. Liu and H. Pan, *ChemistrySelect*, 2017, **2**, 5244–5247.
32 S. H. Kim, L. B. Chen, J. S. Lee, A. Kim, J. M. Seo, J. H. Baek, S. J. Lee, B. J. Jang, C. Li, R. Guan, Y. Shao, J. Li, X. Y. Lang, Y. S. Kim, G. F. Han, Q. Jiang and J. B. Baek, *Adv. Mater.*, 2025, **38**, e11666.
33 V. Martinez, T. Stolar, B. Karadeniz, I. Brekalo and K. Užarević, *Nat. Rev. Chem.*, 2023, **7**, 51–65.
34 P. S. Weiss, *Science*, 2023, **380**, 1013.
35 I. R. Speight, K. J. Ardila-Fierro, J. G. Hernández, F. Emmerling, A. A. L. Michalchuk, F. García, E. Colacino and J. Mack, *Nat. Rev. Methods Primers*, 2025, **5**, 29.
36 S. H. Kim, R. Guan, J. Gu, Y. Shao, Q. Zhao, L. Sheng, J. S. Lee, S. J. Lee, J. H. Baek, C. Li, J. Li, Q. Li, H. Lim and J. B. Baek, *J. Am. Chem. Soc.*, 2025, **147**, 32035–32044.
37 R. Guan, L. Sheng, C. Li, J. Gu, J.-M. Seo, B.-J. Jang, S.-H. Kim, J. Kim, H. Lim, Q. Li and J.-B. Baek, *Nat. Nanotechnol.*, 2025, **20**, 1247–1253.
38 K. Yatagai, Y. Shishido, R. Gemma, T. Boll, H.-H. Uchida and K. Oguri, *Int. J. Hydrogen Energy*, 2020, **45**, 5264–5275.
39 W. Zheng, L. Lei and Y. Hou, *Matter*, 2025, **8**, 102381.
40 P. Baláž, M. Achimovičová, M. Baláž, P. Billik, Z. Cherkezova-Zheleva, J. M. Criado, F. Delogu, E. Dutková, E. Gaffet, F. J. Gotor, R. Kumar, I. Mitov, T. Rojac, M. Senna, A. Streletskii and K. Wieczorek-Ciurowa, *Chem. Soc. Rev.*, 2013, **42**, 7571–7637.
41 K. Lv, W. Lv, C. Liu, C. Liu, M. Claeys, G. Ren, W. Deng and T. Yu, *Chem. Eng. J.*, 2025, **503**, 158301.
42 L. Takacs, *Chem. Soc. Rev.*, 2013, **42**, 7649–7659.
43 S. Mori, W.-C. Xu, T. Ishidzuki, N. Ogasawara and K. K. J. Imai, *Appl. Catal. A: Gen.*, 1996, **137**, 255–268.
44 X. Liu, Y. Li, L. Zeng, X. Li, N. Chen, S. Bai, H. He, Q. Wang and C. Zhang, *Adv. Mater.*, 2022, **34**, 2108327.
45 C. Bolm and J. G. Hernández, *Angew. Chem., Int. Ed.*, 2019, **58**, 3285–3299.

46 R. Guan, H. Zhang, C. Li and J.-B. Baek, *Joule*, 2026, **10**, 102419.
47 Y. Shao, R. Guan, J. Gu, W. Che, C. Li, B.-J. Jang, S.-H. Kim, J. S. Lee, D. Lim, H. Lim, R. Chen and J.-B. Baek, *Joule*, 2026, **10**, 102358.
48 G. F. Han, F. Li, Z. W. Chen, C. Coppex, S. J. Kim, H. J. Noh, Z. Fu, Y. Lu, C. V. Singh, S. Siahrostami, Q. Jiang and J. B. Baek, *Nat. Nanotechnol.*, 2021, **16**, 325–330.
49 H. Shahbeik, S. Hu, S. Motamedi, S. A. F. Sheikh Ahmad Tajuddin, M. Tabatabaei and M. Aghbashlo, *Renew. Sustain. Energy Rev.*, 2026, **226**, 116442.
50 R. Tu, X. Ci, C. Wei, K. Lv, T. Yu and W.-Q. Deng, *Catal. Sci. Technol.*, 2025, **15**, 5938–5949.
51 K. Sawahara, K. Yatagai, T. Boll, A. Pundt and R. Gemma, *Int. J. Hydrogen Energy*, 2022, **47**, 19051–19061.
52 N. Gamba, V. Farina, S. Garroni, G. Mulas and F. Gennari, *Powder Technol.*, 2021, **377**, 857–867.
53 G.-C. Mao, X.-T. Kan, M.-X. Xiao, W.-L. Liu, B.-X. Dong and Y.-L. Teng, *Ind. Eng. Chem. Res.*, 2022, **61**, 10124–10132.
54 R. Tu, Y. Zhang, Y. Xu, J. Yang, L. Zhang, K. Lv, G. Ren, S. Zhai, T. Yu and W. Deng, *Nanoscale Horiz.*, 2023, **8**, 852–858.
55 Y. Sawama, M. Niikawa, K. Ban, K. Park, S.-y. Aibara, M. Itoh and H. Sajiki, *Bull. Korean Chem. Soc.*, 2020, **93**, 1074–1078.
56 F. Torre, V. Farina, A. Taras, C. Pistidda, A. Santoru, J. Bednarcik, G. Mulas, S. Enzo and S. Garroni, *Powder Technol.*, 2020, **364**, 915–923.
57 Z. Ye, F. Huang, L. Wu, S. Wang and L. Zhang, *Fuel*, 2026, **410**, 137952.
58 K. Lv, R. Tu, L. Xiao, W. Wei, Y. Xu, G. Ren, R. Huang, W. Deng and T. Yu, *Chem. Eng. J.*, 2023, **471**, 144613.
59 S. Das, J. Pérez-Ramírez, J. Gong, N. Dewangan, K. Hidajat, B. C. Gates and S. Kawi, *Chem. Soc. Rev.*, 2020, **49**, 2937–3004.
60 Q. Liao, Y. Song, W. Li, D. He, A. Pan and C. Han, *Mater. Sci. Technol.*, 2025, **218**, 108–125.
61 T. Len and R. Luque, *Green Chem.*, 2023, **25**, 490–521.
62 F. Feng, G. Song, J. Xiao, L. Shen and S. V. Pisupati, *Fuel*, 2019, **235**, 85–91.
63 K. Feng, J. Tian, M. Guo, Y. Wang, S. Wang, Z. Wu, J. Zhang, L. He and B. Yan, *Appl. Catal. B Environ.*, 2021, **292**, 120191.
64 K. L. Chagoya, D. J. Nash, T. Jiang, D. Le, S. Alayoglu, K. B. Idrees, X. Zhang, O. K. Farha, J. K. Harper, T. S. Rahman and R. G. Blair, *ACS Sustain. Chem. Eng.*, 2021, **9**, 2447–2455.